photonics

MDPI

Communication

Highly Sensitive Biosensor Based on Partially Immobilized Silver Nanopillars in the Terahertz Band

Shuo Liu [1,2,3,*], Lin Li [1,2,3] and Zhenxu Bai [1,2,3]

[1] Center for Advanced Laser Technology, Hebei University of Technology, Tianjin 300401, China; 184186@stu.hebut.edu.cn (L.L.); zxbai@hebut.edu.cn (Z.B.)
[2] Hebei Key Laboratory of Advanced Laser Technology and Equipment, Tianjin 300401, China
[3] Tianjin Key Laboratory of Electronic Materials and Devices, Tianjin 300401, China
* Correspondence: liushuo@hebut.edu.cn

Abstract: In this paper, a highly sensitive biosensor based on partially immobilized silver nanopillars is proposed. The working frequency of this sensor is in the terahertz band, and the range of the detected refractive index is 1.33 to 1.38. We set air holes of two different sizes on the cross-section of the optical fiber and arranged them into a hexagon. In order to improve the sensitivity, silver nanopillars were immobilized on part of the surface of the fiber cladding. The method for detecting the change of refractive index of the bio-analyte was based on local surface plasmon resonance properties of noble metal. The research recorded valuable data about the values of loss peak and full width at half maximum as well as resonance frequency shift under different setting conditions. The data present the biosensor's final sensitivity as 1.749 THz/RIU.

Keywords: PCF; biosensor; terahertz band; silver nanopillar

Citation: Liu, S.; Li, L.; Bai, Z. Highly Sensitive Biosensor Based on Partially Immobilized Silver Nanopillars in the Terahertz Band. *Photonics* **2021**, *8*, 438. https://doi.org/10.3390/photonics8100438

Received: 24 August 2021
Accepted: 12 October 2021
Published: 13 October 2021

1. Introduction

In the past few decades, due to high performance and simple manufacturing steps of photonic sensors, people have displayed increasing interest in photonic sense solutions [1–4]. Recently, optical technology was developed, which improves the detection limit as well as the sensitivity and the selectivity of biosensors. In the past decades, a variety of optical biosensor methods were developed, including surface plasmon resonance (SPR) [5,6], quartz crystal microbalance [7,8], and ellipsometer [9]. Zhang et al. proposed a dual-channel microfluidic sensor based on a side-hole fiber with the advantage of system integration [10]. Yin et al. proposed an optical fiber sensor-integrated microfluidic chip for ultrasensitive detection of glucose, and the performances in response time and detection range were significantly improved [11]. The integrated solution provides high sensitivity in a small footprint, paving the way for detection and collection of individual particles. Lab-on-a-chip (LOC) is miniaturized integrated equipment that has significant advantages over standard biological detection methods [12]. At the same time, the photonic biosensor has the characteristics of high sensitivity, label-free, and real-time detection, which can meet the "on-chip" detection requirements of an LOC platform. Zinoviev et al. demonstrated the performance of an interferometric device based on integrated bimodal waveguides, which could be further integrated in complete LOC platforms for point-of-care diagnostics [13]. Conteduca et al. proposed an optical tweezer based on photonic crystal cavities for the trapping of individual bacteria, which could achieve analysis and monitoring of susceptibility at the single bacterium level [14]. Dielectric metasurfaces also would be applied in this respect [15]. In general, the fiber-based approach has the advantages of small size, lightweight, anti-electromagnetic interference, in-situ monitoring, etc. In addition, the sensitivity of photonic crystal fiber (PCF) can be improved by optimizing the crystal structure (such as gap and hole size).

Optical fiber biosensors based on SPR are most popular for researchers. They have the characteristics of high precision and real-time analysis [16]. They show impressive commercial value in chemistry, life science, and other fields. Wang et al. proposed a highly sensitive optical fiber SPR biosensor with tilted fiber Bragg grating for the detection of human immunoglobulin [17]. Moreno et al. presented a hybrid tilted fiber grating based on SPR for hemoglobin detection [18]. Wu et al. proposed an SPR biosensor scheme based on air/MoS_2/Al/MoS_2-graphene hybrid structure, and the maximum sensitivity was −190.83°/RIU [19]. Wang et al. proposed an SPR biosensor for specific detection of C-reactive protein (CRP) [20]. Aray et al. proposed a plastic optical fiber biosensor based on SPR for the detection of CRP in serum [21]. Dash et al. proposed a biosensor based on PCF made of polymethyl methacrylate using SPR; the refractive index (RI) sensitivity was 2000 nm/RIU [22]. Wu et al. described an ultrasensitive SPR biosensor for detecting carcinoembryonic antigen [23]. Therefore, the SPR biosensor is widely used in the detection of biomarkers worldwide as a reliable, rapid, and accurate analysis method.

A terahertz (THz) band is between infrared and millimeter wave, which is widely used in scientific research, biomedical purposes, and national defense security [24]. The THz band biosensor is sensitive to the local enhancement of electromagnetic fields and the dielectric properties of the surrounding environment at fixed analyte thickness, which can be used for label-free biological detection [25–27]. Mou et al. introduced a THz band PCF for environmental pollutants detection showing the identification of evanescent substances with high sensitivity, and the detection rate of analytes for different applications was 89%~91.5% [28]. Rahman et al. proposed an octagonal-shaped hollow core with eight head star cladding structured PCF sensors for cholesterol detection in human blood and liquid foodstuffs; it showed a sensitivity distribution of 98.75% at 2.2 THz [29]. Zhang et al. reported a metamaterial-based THz biosensor for label-free measurements on cell apoptosis [30]. Sultana et al. proposed a novel Zeonex-based PCF for ethanol detection in the THz frequency range [31].

It is a trend to use metal film coating technology to stimulate SPR to manufacture PCF sensors. When plasma-active metal layers are combined with this structure, their sensing capabilities reach a new height. In 2014, Biswas et al. reported a hollow-core PCF with embedded silver wires for measurement of biofluid. This sensor showed a sensitivity of 2151 nm/RIU for analytes having an RI lower than 1.26 [32]. Klantsataya et al. reported an exposed core microstructure optical fiber with silver film, which achieved an RI sensitivity of 1800 nm/RIU in the sensing range of an aqueous environment (1.33–1.37) suitable for biosensing applications [33]. Zhao et al. demonstrated an SPR refraction sensor based on a side-polished single-mode fiber coated with thin silver film on the flat surface of the optical fiber. It showed a maximum sensitivity of 4365.5 nm/RIU [34]. Abdullah et al. proposed a high sensitivity gold coated circular nano-film PCF biosensor showing the maximum sensitivity response of 45,003.05 nm/RIU for the operated analyte of 1.33–1.40 [35]. To meet the requirements for high throughput and label-free analysis in the diagnostics, optical fiber nano-biosensors using metal nanoparticles to monitor the biomolecular parameters with plentiful sensing performances have been in development for decades [36]. The localized surface plasmon resonance (LSPR) technology has the advantages of enhanced robust sensing and high sensitivity, thereby providing better performance than commercial SPR technology [37]. Sharma et al. presented an LSPR-based biosensor containing gold nanopillar (AuNPL) on an optical fiber substrate to detect glutamate concentrations, and the biosensor achieved a sensitivity of 0.0048 AU/mM [38]. Kumar et al. developed a tapered optical fiber-based sensor probe using AuNPs and cholesterol oxidase to improve sensor sensitivity and selectivity, which showed a sensitivity of 0.125%/mM [39]. Jin et al. presented an LSPR-based biosensor chip and optical fiber of immobilizing AuNPLs onto the surface of polymer substrates [40]. The silver nanopillar (AgNPL) is also one of the best plasma candidates for LSPR-based nano-biosensors that have been used to detect a variety of analytes, including enzymes, chemicals, and metal ions [41]. Agrawal et al. proposed an optical fiber sensor fabricated and immobilized with

AgNPLs and functionalized with polyethylene glycol to detect dopamine [42]. Wang et al. developed an AgNPL-based SPR biosensor for sensitive detection of microRNA without the biomodification on amplification tags [43]. Compared with metal film, optical fiber immobilized with metal nanoparticle is more sensitive in detecting small changes in RI.

In this study, we characterized a THz optical fiber biosensor partially immobilized with AgNPLs based on SPR. Through the extrusion of the large air holes on both sides of the fiber core, the energy was more easily transferred to the periphery of AgNPLs, resulting in an SPR effect. In order to find the best structural conditions with high relative sensitivity and ease of measure, we changed the size of the air holes on cladding and the size of the AgNPLs.

2. Structural Design and Materials

Figure 1 shows the cross-section of the highly sensitive biosensor based on partially immobilized AgNPLs on the cladding surface. The cross-section of the biosensor is revealed in Figure 1a. The cladding material was polycarbonate (PC) (the RI is 1.66), which allowed light in the THz band to pass through [44]. In the figure, the purplish areas refer to small air holes, and the green areas refer to large air holes. They wware regularly distributed in two layers in a hexagonal shape. As shown in Figure 1a, the outer layer is composed of eleven small air holes with a radius of r_1, and an air hole near the silver layer (yellow part) was deleted. Compared to existing the air hole, deleting allowed the energy of the core to more fully contact the AgNPLs without hindrance, achieving a stronger SPR effect. The inner layer was composed of four small air holes and two large air holes with r_2, and the two large air holes were symmetrically distributed on the horizontal center of the entire fiber section. The spacing of all air holes was Λ = 65 μm. The radius of cladding R = 320 μm, and the yellow area on the cladding surface represents AgNPLs, whose local enlarged view is shown in Figure 1b. The AgNPLs were immobilized neatly on one-sixth of the surface of the fiber cladding, which was close to the deleted air hole, and the distance between a single AgNPL could not exceed 1 μm. Extending from the surface of the cladding was the analyte layer (50 μm) and the perfectly matched layer (50 μm) in turn. They are represented by the cyan area and the blue area, respectively. The permittivity of Ag refers to Drude model dielectric function [45]:

$$\varepsilon_{\text{Drude}} = 1 - \frac{\omega_P}{\omega^2 - j\omega_\tau \omega} \tag{1}$$

where ω_p is the plasma frequency and ω_τ is the damping frequency. As for silver, $\omega_p = 1.37 \times 10^{16}$ (rad/s) and $\omega_\tau = 2.733 \times 10^{13}$ (rad/s) in the THz band. The electric field energy distribution of the SPP mode is demonstrated in Figure 1c. The energy was evenly distributed around the AgNPLs. The region closer to the individual AgNPL had the higher energy on account of SPR properties of noble metal nanoparticles.

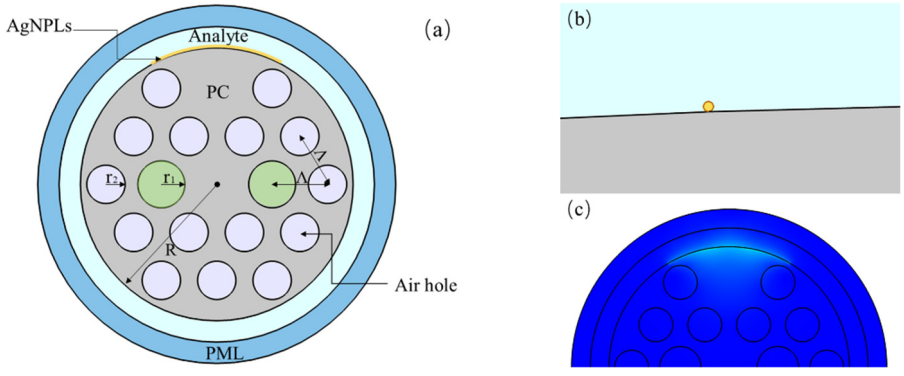

Figure 1. (**a**) The cross-section of PCF, (**b**) the schematic diagram of AgNPLs, (**c**) SPP mode.

The PC is an engineering plastic with excellent transparency and impact strength. The main advantage of using this material for optical fiber manufacturing lies in the well-balanced combination of optical and mechanical properties. Fasano et al. used the PC to make a solid-core microstructure polymer optical fiber with a final fiber diameter of approximately 150 μm and a core diameter of 7 μm [46]. Dadabayev et al. proposed an RGB demultiplexer based on the PC multicore polymer optical fiber structure [47]. The manufacturing process of the optical fiber needs two steps. The first step is to use plastic pellets to cast solid PC rods. When casting solid rods, the PC pellets need to be dried before casting. Bubble formation needs to be avoided, otherwise it increases transmission loss and reduces the mechanical properties of the final fiber. The second step is to use drilling and drawing techniques to manufacture PCF. When the solid rod is machined, the required hole pattern is drilled in it, and the hole pattern is composed of two types of air holes. The preform is finally drawn into a middle cane, which is then sheathed with an internally manufactured PC tube and drawn into fibers.

There are many examples of immobilizing silver on plastic optical fiber (POF). Sultangazin et al. fabricated a POF sensor for hydrogen sulfide detection through silver deposition on the POF outer surface [48]. Grassini et al. described a POF sensor suitable for measuring low concentrations of pollutants in the atmosphere, and silver was deposited on POF by direct current sputtering [49]. Shobin et al. coated silver nanowires on PMMA fibers using dip coating technique [50]. In this work, AgNPLs could be immobilized on the surface of optical fiber cladding by means of the dip coating technique.

The measurable RI range of the analyte is from 1.33 to 1.38 because the RI of most biomolecular materials, such as cypton, plasma, and hemoglobin, is between 1.33 and 1.38 [51]. Nano-silver can bind with some biomolecules such as hemoglobin, and the binding affinity between nano-silver and hemoglobin increases with the increase of temperature (from room temperature to 42 °C) [52], thus the sensor has a stronger detection ability for sulfur-containing proteins. Liu et al. proposed a THz SPR biosensor for detecting blood components. Its sensitivity is linear in the RI range of 1.33–1.38 [53]. Arunkumar et al. used a second dimension photonic crystal based biosensor to detect the RIs of cypton, blood plasma, and hemoglobin, which were 1.34, 1.35, and 1.38, respectively [54]. The proposed biosensor can detect analytes repeatedly. After a biomolecular detection, the biosensor is cleaned with deionized water to remove the bound biomolecular and then rinsed with phosphate buffered saline before starting of next measurement [55]. The next section explores the influence of different structure parameters on the location and the value of loss peak. Parameters to be changed were the radius of big air holes, the radius of small air holes, and the radius of the AgNPLs. We calculated the loss peaks of the PCF fundamental mode at the analyte RIs of 1.33 and 1.38 under different values of each parameter.

3. Optimization Process

Initially, we set the parameters of the biosensor structure to r_1 = 60 μm, R_{Ag} = 100 nm, r_2 = 40 μm. Then, we changed the parameter values in the order of r_1, $R_{Ag,}$ and r_2 and got the optimal value under each parameter condition in turn. In the optimization process, we used the finite element method to solve the model.

Firstly, we changed the value of parameter r_1, selected the big air hole radius r_{1s} as 55 μm, 60 μm, 65 μm, and 70 μm for analysis, while other structure parameters of the optical fiber sensor remained unchanged. As Figure 2a shows, when the RI of bioanalyte was 1.33, the resonance frequencies of the biosensor were respectively 1.141 THz, 1.199 THz, 1.255 THz, and 1.327 THz; correspondingly, the maximum losses were 1088.09 dB/m, 755.27 dB/m, 592.88 dB/m, and 487.81 dB/m. When the RI of bioanalyte was 1.38, the resonance frequencies were 1.24 THz, 1.3 THz, 1.369 THz, and 1.452 THz, and the maximum losses were 614.23 dB/m, 476.08 dB/m, 384.79 dB/m, and 333.60 dB/m. The resonance frequency shifts corresponding to two RIs of analyte were 0.099 THz, 0.101 THz, 0.114 THz, and 0.125 THz. The results in Figure 2b showed that the larger r_1 was, the greater was the deviation of its resonance frequency. However, as the air hole became larger, the loss

peak value gradually decreased, and full width at half maximum (FWHM) of loss curves was wider in the RIs of bioanalyte of 1.33 to 1.38. It had the maximum shift but unsuitable FWHM and loss peak when r_1 = 70 μm. Taking into consideration the loss peak and the FWHM, we chose the parameter r_1 = 55 μm with suitable resonance frequency shift for the largest loss peak value and the narrowest FWHM.

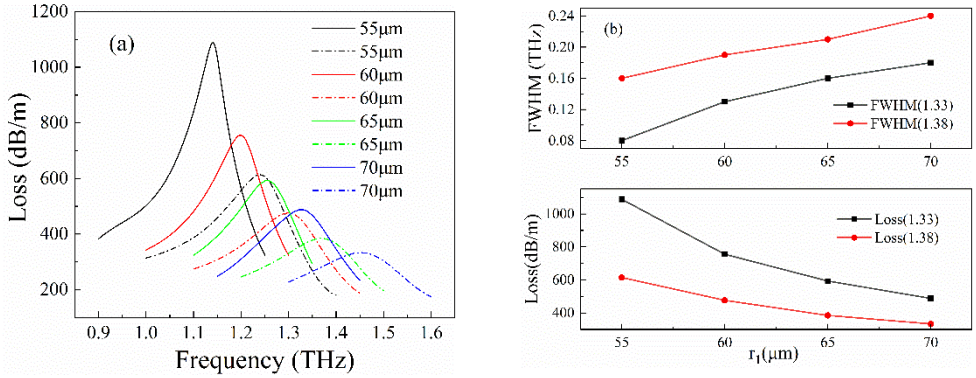

Figure 2. (**a**) Loss peak curves of different r_1, solid line (the RI of bioanalyte is 1.33) and dashed line (the RI of bioanalyte is 1.38). (**b**) FWHM and loss of different r_1.

Under the condition of r_1 = 55 μm, we optimized the radius of AgNPLs as given by R_{Ag}. Then, we selected R_{Ags} as 80 nm, 90 nm, 100 nm, and 110 nm to calculate the fundamental loss at two different RIs of bioanalyte. In Figure 3a, as R_{Ag} increased, the resonance frequency shifts corresponding to RIs of two analytes were almost the same, while the value of loss peak was increasing. As the results in Figure 3b show, there were maximum loss peaks of 1535.53 dB/m and 768.99 dB/m in the RIs of both 1.33 and 1.38 when R_{Ag} = 110 nm. For R_{Ag} = 80 nm, the corresponding two loss values were 651.34 dB/m and 432.23 dB/m. When R_{Ag} = 110 nm, the FWHM was the narrowest, but the loss peak attenuation was too large between the two different RIs, thus we did not make this value the first choice. Considering the above three aspects comprehensively, we chose 100 nm as the optimal radius of AgNPLs because of its high loss peak, narrow FWHM, and obvious resonance frequency shift.

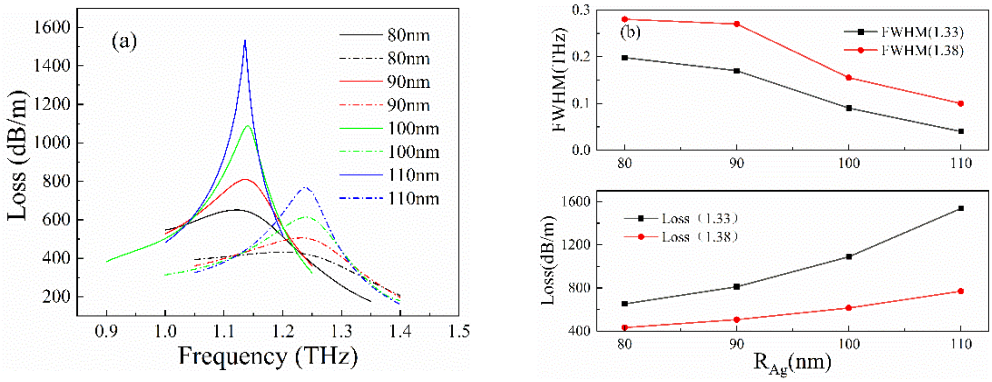

Figure 3. (**a**) Loss peak curves of different R_{Ag}. (**b**) FWHM and loss of different R_{Ag}.

Based on the above two optimized parameters, we carried out the following optimization process to get the most suitable small air hole size. r_{2s} were set as 35 μm, 40 μm, 45 μm, and 50 μm. The calculation results were illustrated in Figure 4. As we can see from Figure 4a, the influence of changing r_2 on the loss peak was not as great as r_1 and R_{Ag}. Figure 4b illustrates some concrete data showing the RI of bioanalyte was 1.33, the FWHM values were 0.12 THz, 0.09 THz, 0.06 THz, and 0.045 THz, which correspondingly

were 0.175 THz, 0.2 THz, 0.13 THz, and 0.1 THz when the RI of bioanalyte was 1.38. The optical fiber had the largest loss peak and the narrowest FWHM with r_2 = 50 µm, while that with r_2 = 35 µm was the opposite, thus we choose the best value from 45 µm and 50 µm. As r_2 increased, the position of the loss peak moved to a lower frequency band. When r_2 = 45 µm and 50 µm, the shifts of the resonance frequency were 0.085 THz and 0.075 THz, respectively, and were larger when r_2 = 45 µm. As a result, we chose r_2 = 45 µm as the optimal value.

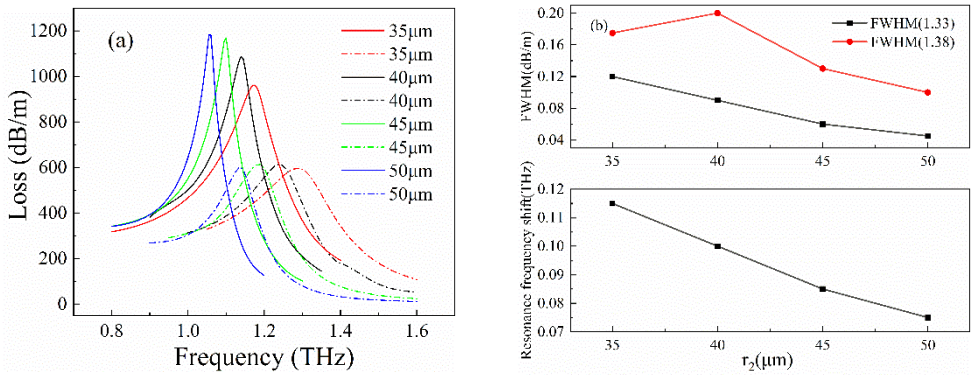

Figure 4. (**a**) Loss peak curves of different r_2. (**b**) FWHM and resonance frequency shift of different r_2.

4. Sensing Analysis

Finally, we chose r_1 = 55 µm, R_{Ag} = 100 nm, and r_2 = 45 µm as the optimal biosensor structure. Then, we selected six values at equal intervals from 1.33 to 1.38 as the RIs of bioanalyte and calculated the loss under different RIs. The results were shown in Figure 5. When the RI of bioanalyte increased, the resonance frequency of the fiber moved to a larger frequency band. Observing the graph, we can find that the value of the loss peak became smaller, from 1011.89 dB/m to 615.99 dB/m.

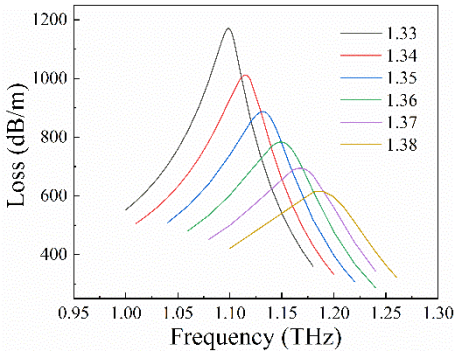

Figure 5. Loss peak curves with different RI of bioanalyte.

Figure 6 shows the RI curve of PCF. We fabricated a device based on the optimized fiber structure and tested bioanalyte with different RIs. When the bioanalyte RI was in the range of 1.33 to 1.38, the shift of the resonance frequency was in the range of 1.099 THz to 1.186 THz. As a result, the sensitivity of this biosensor was 1.749 THz/RIU (corresponding to 230,164 nm/RIU). Compared with current biosensors of the same type, it shows great advantages in terms of high sensitivity. Figure 6 represents that there is strong linearity between the RI and the resonance frequency when the RI of the bioanalyte was between 1.33 and 1.38. The fitted curve expression is:

$$y = 1.749x - 1.228 \quad (2)$$

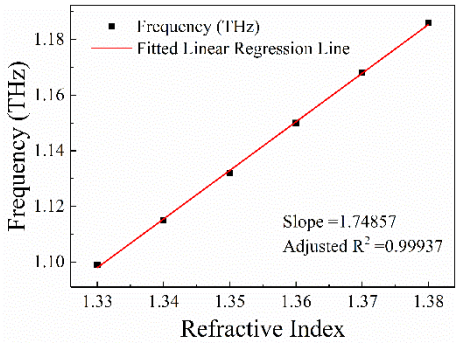

Figure 6. Variation of resonance frequency with different RIs of bioanalyte.

Furthermore, there were small residual errors between the experimental values and the fitting values. Therefore, the fitted curve matches the experimental trend well.

Table 1 presents the respective comparison of the proposed biosensor to the representative biosensor based on SPR and integrated biosensors reported previously. According to the table, the wavelength sensitivity of biosensor using silver to excite SPR effect was higher than that using gold. Furthermore, the biosensors with SPR excited by metal nanoparticles had a better performance than those excited by metal film. The proposed sensor used AgNPLs as the excitation material, and the wavelength sensitivity was 230,164 nm/RIU, which is far better than previous sensors of the same type. It proves the great superiority of AgNPLs in biological detection. However, there is no doubt that integrated biosensors are portable, easy-to-use and have great advantages in real-time detection. It will have a very positive impact on our lifestyle.

Table 1. Comparison table of the performance of the proposed biosensor and other counterparts reported in literature.

Sensor Configuration/Materials Coating	Type of Excitation	Sensitivity	Working Band	Ref
PCF/gold film	SPR	2200 nm/RIU	0.6–0.652 μm	[56]
PCF/gold film	SPR	3435 nm/RIU	575–815 nm	[57]
PCF/gold nanoparticles	LSPR	3915 nm/RIU	656–813 nm	[58]
SP-SMF/silver film	SPR	4365.5 nm/RIU	508–731 nm	[34]
PCF/silver nanowires	LSPR	9000 nm/RIU	599–768 nm	[59]
Microring resonator	/	80 nm/RIU	~850 nm	[60]
GMR sensor	/	186 nm /RIU	841–863 nm	[61]
This paper	LSPR	230,164 nm/RIU	253–273 μm	

5. Conclusions

In conclusion, we designed and studied a biosensor partially immobilized with AgNPLs on the surface of optical fiber cladding, which can be used to detect most biomolecular solutions in the THz range. The sensitivity of the proposed PCF was evaluated by using glycerol aqueous solution. The results show that the sensitivity of 1.749 THz/RIU was obtained as the bioanalyte in the refractive index range of 1.33 to 1.38. It shows the great advantages of being a partially immobilized metal particle structure. Therefore, the proposed biosensor has excellent reliability in biomedical applications with high sensitivity.

Author Contributions: Conceptualization, S.L.; software, L.L.; formal analysis, Z.B.; writing—original draft preparation, L.L. and S.L. All authors have read and agreed to the published version of the manuscript.

Funding: This research was funded by National Science Foundation of China grant number 61805067, 61905061; Science and Technology Research Project of Hebei Province Higher Education grant number BJ2018047; Natural Science Foundation of Hebei Province grant number F2020202069.

Institutional Review Board Statement: Not applicable.

Informed Consent Statement: Not applicable.

Conflicts of Interest: The authors declare no conflict of interest.

References

1. Lyu, C.; Liu, Z.; Huo, Z.; Ge, C.; Cheng, X.; Tam, H.-Y. High-sensitivity, high-spatial-resolution distributed strain sensing based on a poly(methyl methacrylate) chirped fiber Bragg grating. *Photon. Res.* **2020**, *8*, 1134–1139. [CrossRef]
2. Shen, L.; Wu, H.; Zhao, C.; Shen, L.; Zhang, R.; Tong, W.; Fu, S.; Research, M.T.J.P. Distributed curvature sensing based on a bending loss-resistant ring-core fiber. *Photon. Res.* **2020**, *8*, 165. [CrossRef]
3. Sun, C.T.; Wang, R.; Jin, X.R.; Wang, Z.M.; Liu, W.L.; Zhang, S.; Ma, Y.W.; Lin, J.Y.; Li, Y.; Geng, T.; et al. A new phase-shifted long-period fiber grating for simultaneous measurement of torsion and temperature. *Chin. Opt. Lett.* **2020**, *18*, 021203. [CrossRef]
4. Cao, L.; Yu, Y.; Xiao, M.; Yang, J.B.; Zhang, X.L.; Meng, Z. High sensitivity conductivity-temperature-depth sensing based on an optical microfiber coupler combined fiber loop. *Chin. Opt. Lett.* **2020**, *18*, 011202. [CrossRef]
5. Zhou, J.; Qi, Q.; Wang, C.; Qian, Y.; Liu, G.; Wang, Y.; Fu, L. Surface plasmon resonance (SPR) biosensors for food allergen detection in food matrices. *Biosens. Bioelectron.* **2019**, *142*, 111449. [CrossRef] [PubMed]
6. Falkowski, P.; Lukaszewski, Z.; Gorodkiewicz, E. Potential of surface plasmon resonance biosensors in cancer detection. *J. Pharm. Biomed. Anal.* **2021**, *194*, 113802. [CrossRef] [PubMed]
7. Saad, N.A.; Zaaba, S.K.; Zakaria, A.; Kamarudin, L.M.; Wan, K.; Shariman, A.B. Quartz crystal microbalance for bacteria application review. In Proceedings of the 2014 2nd International Conference on Electronic Design (ICED), Penang, Malaysia, 19–21 August 2014; pp. 455–460.
8. Atashbar, M.Z.; Bejcek, B.; Vijh, A.; Singamaneni, S. QCM biosensor with ultra thin polymer film. *Sens. Actuators B Chem.* **2005**, *107*, 945–951. [CrossRef]
9. Arwin, H. Spectroscopic ellipsometry and biology: Recent developments and challenges. *Thin Solid Film.* **1998**, *313–314*, 764–774. [CrossRef]
10. Zhang, Y.; Li, Y.Z.; Liu, C.; Liu, Z.H.; Zhang, Y.X.; Yang, X.H.; Zhang, J.Z.; Yang, J.; Yuan, L.B. Dual-channel microfluidic sensor based on side-hole fiber with two long-period fiber gratings. *Chin. Opt. Lett.* **2020**, *18*. [CrossRef]
11. Yin, M.-J.; Huang, B.; Gao, S.; Zhang, A.P.; Ye, X. Optical fiber LPG biosensor integrated microfluidic chip for ultrasensitive glucose detection. *Biomed. Opt. Express* **2016**, *7*, 2067–2077. [CrossRef]
12. Estevez, M.C.; Alvarez, M.; Lechuga, L.M. Integrated optical devices for lab-on-a-chip biosensing applications. *Laser Photonics Rev.* **2012**, *6*, 463–487. [CrossRef]
13. Zinoviev, K.E.; Gonzalez-Guerrero, A.B.; Dominguez, C.; Lechuga, L.M. Integrated bimodal waveguide interferometric biosensor for label-free analysis. *J. Lightwave Technol.* **2011**, *29*, 1926–1930. [CrossRef]
14. Conteduca, D.; Brunetti, G.; Dell'Olio, F.; Armenise, M.N.; Krauss, T.F.; Ciminelli, C. Monitoring of individual bacteria using electro-photonic traps. *Biomed. Opt. Express* **2019**, *10*, 3463–3471. [CrossRef] [PubMed]
15. Algorri, J.F.; Zografopoulos, D.C.; Ferraro, A.; García-Cámara, B.; Beccherelli, R.; Sánchez-Pena, J.M. Ultrahigh-quality factor resonant dielectric metasurfaces based on hollow nanocuboids. *Opt. Express* **2019**, *27*, 6320–6330. [CrossRef]
16. Singh, P. SPR biosensors: Historical perspectives and current challenges. *Sens. Actuators B Chem.* **2016**, *229*, 110–130. [CrossRef]
17. Wang, Q.; Jing, J.; Wang, B. Highly sensitive SPR biosensor based on graphene oxide and staphylococcal protein a Co-Modified TFBG for human IgG detection. *IEEE Trans. Instrum. Meas.* **2019**, *68*, 3350–3357. [CrossRef]
18. Moreno, Y.; Song, Q.; Xing, Z.; Sun, Y.; Letters, Z.Y.J.C.O. Hybrid tilted fiber gratings-based surface plasmon resonance sensor and its application for hemoglobin detection. *Chin. Opt. Lett.* **2020**, *18*, 100601. [CrossRef]
19. Wu, L.; Jia, Y.; Jiang, L.; Guo, J.; Dai, X.; Xiang, Y.; Fan, D. Sensitivity improved SPR biosensor based on the MoS2/graphene–aluminum hybrid structure. *J. Lightwave Technol.* **2017**, *35*, 82–87. [CrossRef]
20. Wang, W.; Mai, Z.; Chen, Y.; Wang, J.; Li, L.; Su, Q.; Li, X.; Hong, X. A label-free fiber optic SPR biosensor for specific detection of C-reactive protein. *Sci. Rep.* **2017**, *7*, 16904. [CrossRef]
21. Aray, A.; Chiavaioli, F.; Arjmand, M.; Trono, C.; Tombelli, S.; Giannetti, A.; Cennamo, N.; Soltanolkotabi, M.; Zeni, L.; Baldini, F. SPR-based plastic optical fibre biosensor for the detection of C-reactive protein in serum. *J. Biophotonics* **2016**, *9*, 1077–1084. [CrossRef]
22. Dash, J.N.; Jha, R. SPR biosensor based on polymer PCF coated with conducting metal oxide. *IEEE Photonics Technol. Lett.* **2014**, *26*, 595–598. [CrossRef]
23. Wu, Q.; Li, N.; Wang, Y.; Liu, Y.; Xu, Y.; Wei, S.; Wu, J.; Jia, G.; Fang, X.; Chen, F.; et al. A 2D transition metal carbide MXene-based SPR biosensor for ultrasensitive carcinoembryonic antigen detection. *Biosens. Bioelectron.* **2019**, *144*, 111697. [CrossRef]
24. Menikh, A.; MacColl, R.; Mannella, C.A.; Zhang, X.-C. Terahertz biosensing technology: Frontiers and progress. *ChemPhysChem* **2002**, *3*, 655–658. [CrossRef]
25. Markelz, A.G. Terahertz dielectric sensitivity to biomolecular structure and function. *IEEE J. Sel. Top. Quantum Electron.* **2008**, *14*, 180–190. [CrossRef]
26. Lee, D.K.; Kim, G.; Kim, C.; Jhon, Y.M.; Kim, J.H.; Lee, T.; Son, J.H.; Seo, M. Ultrasensitive detection of residual pesticides using THz near-field enhancement. *IEEE Trans. Terahertz Sci. Technol.* **2016**, *6*, 389–395. [CrossRef]
27. Saadeldin, A.S.; Hameed, M.F.O.; Elkaramany, E.M.A.; Obayya, S.S.A. Highly sensitive terahertz metamaterial sensor. *IEEE Sens. J.* **2019**, *19*, 7993–7999. [CrossRef]

28. Mou, F.A.; Rahman, M.M.; Islam, M.R.; Bhuiyan, M.I.H. Development of a photonic crystal fiber for THz wave guidance and environmental pollutants detection. *Sens. Bio-Sens. Res.* **2020**, *29*, 100346. [CrossRef]
29. Rahman, M.M.; Mou, F.A.; Bhuiyan, M.I.H.; Islam, M.R. Photonic crystal fiber based terahertz sensor for cholesterol detection in human blood and liquid foodstuffs. *Sens. Bio-Sens. Res.* **2020**, *29*, 100356. [CrossRef]
30. Zhang, C.; Liang, L.; Ding, L.; Jin, B.; Hou, Y.; Li, C.; Jiang, L.; Liu, W.; Hu, W.; Lu, Y.; et al. Label-free measurements on cell apoptosis using a terahertz metamaterial-based biosensor. *Appl. Phys. Lett.* **2016**, *108*, 241105. [CrossRef]
31. Sultana, J.; Islam, M.S.; Ahmed, K.; Dinovitser, A.; Ng, B.W.H.; Abbott, D. Terahertz detection of alcohol using a photonic crystal fiber sensor. *Appl. Opt.* **2018**, *57*, 2426–2433. [CrossRef]
32. Biswas, T.; Chattopadhyay, R.; Bhadra, S.K. Plasmonic hollow-core photonic band gap fiber for efficient sensing of biofluids. *J. Opt.* **2014**, *16*, 045001. [CrossRef]
33. Klantsataya, E.; François, A.; Ebendorff-Heidepriem, H.; Hoffmann, P.; Monro, T.M. Surface plasmon scattering in exposed core optical fiber for enhanced resolution refractive index sensing. *Sensors* **2015**, *15*, 25090–25102. [CrossRef] [PubMed]
34. Zhao, J.; Cao, S.; Liao, C.; Wang, Y.; Wang, G.; Xu, X.; Fu, C.; Xu, G.; Lian, J.; Wang, Y. Surface plasmon resonance refractive sensor based on silver-coated side-polished fiber. *Sens. Actuators B Chem.* **2016**, *230*, 206–211. [CrossRef]
35. Abdullah, H.; Ahmed, K.; Mitu, S.A. Ultrahigh sensitivity refractive index biosensor based on gold coated nano-film photonic crystal fiber. *Results Phys.* **2020**, *17*, 103151. [CrossRef]
36. Jeong, H.-H.; Erdene, N.; Park, J.-H.; Jeong, D.-H.; Lee, H.-Y.; Lee, S.-K. Real-time label-free immunoassay of interferon-gamma and prostate-specific antigen using a Fiber-Optic Localized Surface Plasmon Resonance sensor. *Biosens. Bioelectron.* **2013**, *39*, 346–351. [CrossRef] [PubMed]
37. Unser, S.; Bruzas, I.; He, J.; Sagle, L. Localized surface plasmon resonance biosensing: Current challenges and approaches. *Sensors* **2015**, *15*, 15684–15716. [CrossRef] [PubMed]
38. Sharma, P.; Semwal, V.; Gupta, B.D. Highly sensitive and selective localized surface plasmon resonance biosensor for detecting glutamate realized on optical fiber substrate using gold nanoparticles. *Photonics Nanostruct.—Fundam. Appl.* **2019**, *37*, 100730. [CrossRef]
39. Kumar, S.; Kaushik, B.K.; Singh, R.; Chen, N.-K.; Yang, Q.S.; Zhang, X.; Wang, W.; Zhang, B. LSPR-based cholesterol biosensor using a tapered optical fiber structure. *Biomed. Opt. Express* **2019**, *10*, 2150–2160. [CrossRef]
40. Jin, Y.; Wong, K.H.; Granville, A.M. Developing localized surface plasmon resonance biosensor chips and fiber optics via direct surface modification of PMMA optical waveguides. *Colloids Surf. A Physicochem. Eng. Asp.* **2016**, *492*, 100–109. [CrossRef]
41. Amirjani, A.; Haghshenas, D.F. Ag nanostructures as the surface plasmon resonance (SPR)-based sensors: A mechanistic study with an emphasis on heavy metallic ions detection. *Sens. Actuators B: Chem.* **2018**, *273*, 1768–1779. [CrossRef]
42. Agrawal, N.; Zhang, B.; Saha, C.; Kumar, C.; Kaushik, B.K.; Kumar, S. Development of dopamine sensor using silver nanoparticles and PEG-functionalized tapered optical fiber structure. *IEEE Trans. Biomed. Eng.* **2020**, *67*, 1542–1547. [CrossRef] [PubMed]
43. Wang, X.; Hou, T.; Lin, H.; Lv, W.; Li, H.; Li, F. In situ template generation of silver nanoparticles as amplification tags for ultrasensitive surface plasmon resonance biosensing of microRNA. *Biosens. Bioelectron.* **2019**, *137*, 82–87. [CrossRef] [PubMed]
44. Piesiewicz, R.; Jansen, C.; Wietzke, S.; Mittleman, D.; Koch, M.; Kürner, T.J.I.J.o.I.; Waves, M. Properties of building and plastic materials in the THz range. *Int. J. Infrared Millim. Waves* **2007**, *28*, 363–371. [CrossRef]
45. Hosseininejad, S.E.; Komjani, N. Waveguide-fed tunable terahertz antenna based on hybrid graphene-metal structure. *IEEE Trans. Antennas Propag.* **2016**, *64*, 3787–3793. [CrossRef]
46. Fasano, A.; Woyessa, G.; Stajanca, P.; Markos, C.; Stefani, A.; Nielsen, K.; Rasmussen, H.K.; Krebber, K.; Bang, O. Fabrication and characterization of polycarbonate microstructured polymer optical fibers for high-temperature-resistant fiber Bragg grating strain sensors. *Opt. Mater. Express* **2016**, *6*, 649–659. [CrossRef]
47. Dadabayev, R.; Malka, D. A visible light RGB wavelength demultiplexer based on polycarbonate multicore polymer optical fiber. *Opt. Laser Technol.* **2019**, *116*, 239–245. [CrossRef]
48. Sultangazin, A.; Kusmangaliyev, J.; Aitkulov, A.; Akilbekova, D.; Olivero, M.; Tosi, D. Design of a smartphone plastic optical fiber chemical sensor for hydrogen sulfide detection. *IEEE Sens. J.* **2017**, *17*, 6935–6940. [CrossRef]
49. Grassini, S.; Ishtaiwi, M.; Parvis, M.; Vallan, A. Design and deployment of low-cost plastic optical fiber sensors for gas monitoring. *Sensors* **2015**, *15*, 485–498. [CrossRef]
50. Shobin, L.R.; Sastikumar, D.; Manivannan, S. Glycerol mediated synthesis of silver nanowires for room temperature ammonia vapor sensing. *Sens. Actuators A Phys.* **2014**, *214*, 74–80. [CrossRef]
51. Yaşlı, A.; Ademgil, H. Modeling the photonic crystal fiber based surface plazmon resonance biosensor to detect blood components. In Proceedings of the 2021 29th Signal Processing and Communications Applications Conference (SIU), Istanbul, Turkey, 9–11 June 2021; pp. 1–4.
52. Zolghadri, S.; Saboury, A.A.; Golestani, A.; Divsalar, A.; Rezaei-Zarchi, S.; Moosavi-Movahedi, A.A. Interaction between silver nanoparticle and bovine hemoglobin at different temperatures. *J. Nanoparticle Res.* **2008**, *11*, 1751. [CrossRef]
53. Liu, S.; Ma, R.; Li, Y.; Zhao, L.; Xia, Y.; Dong, X.; Pang, Y. D-shaped surface plasmon resonance biosensor based on MoS2 in terahertz band. *Opt. Fiber Technol.* **2021**, *66*, 102631. [CrossRef]
54. Arunkumar, R.; Suaganya, T.; Robinson, S.J.P.S. Design and analysis of 2D photonic crystal based biosensor to detect different blood components. *Photonic Sens.* **2019**, *9*, 69–77. [CrossRef]

55. Sridevi, S.; Vasu, K.S.; Sampath, S.; Asokan, S.; Sood, A.K. Optical detection of glucose and glycated hemoglobin using etched fiber Bragg gratings coated with functionalized reduced graphene oxide. *J. Biophotonics* **2016**, *9*, 760–769. [CrossRef] [PubMed]
56. Hasan, M.R.; Akter, S.; Rifat, A.A.; Rana, S.; Ali, S. A highly sensitive gold-coated photonic crystal fiber biosensor based on surface plasmon resonance. *Photonics* **2017**, *4*, 18. [CrossRef]
57. Tong, K.; Wang, F.; Wang, M.; Dang, P.; Wang, Y. Three-core photonic crystal fiber surface plasmon resonance sensor. *Opt. Fiber Technol.* **2018**, *46*, 306–310. [CrossRef]
58. Wang, B.; Wang, Q. Sensitivity-enhanced optical fiber biosensor based on coupling effect between SPR and LSPR. *IEEE Sens. J.* **2018**, *18*, 8303–8310. [CrossRef]
59. Shengxi, J.; Sanfeng, G.; Hanrui, Y.; Hairui, F. Research on dual-core photonic crystal fiber based on local surface plasmon resonance sensor with silver nanowires. *J. Nanophotonics* **2018**, *12*, 1–15. [CrossRef]
60. Samusenko, A.; Gandolfi, D.; Pucker, G.; Chalyan, T.; Guider, R.; Ghulinyan, M.; Pavesi, L. A SiON microring resonator-based platform for biosensing at 850 nm. *J. Lightwave Technol.* **2016**, *34*, 969–977. [CrossRef]
61. Tsai, M.-Z.; Hsiung, C.-T.; Chen, Y.; Huang, C.-S.; Hsu, H.-Y.; Hsieh, P.-Y. Real-time CRP detection from whole blood using micropost-embedded microfluidic chip incorporated with label-free biosensor. *Analyst* **2018**, *143*, 503–510. [CrossRef] [PubMed]